Effects of Additional Layer(s) on the Mobility of Arsenic from Hydrothermally Altered Rock in Laboratory Column Experiments

P. Tangviroon, R. Hayashi, T. Igarashi

Abstract

Hydrothermally altered rocks are frequently encountered when tunnels are constructed in Hokkaido, Japan. High concentrations of hazardous elements, such as arsenic (As), are often released from these rocks into the surrounding environments. Therefore, the rocks are considered potentially hazardous waste. This article describes the effects of water content and oxygen (O_2) concentration in relation to additional layer(s), i.e., surface covering and bottom adsorption layers, on As leaching by using laboratory columns with water content and O_2 concentration sensors. The results show that the use of additional layer(s) has a significant effect on lowering As migration. This was due not only to the adsorption capacity of As by the adsorption layer but also to the water content and O_2 concentration inside the rock layer. The accumulation of pore water was increased in the rock layer in cases with additional layer(s), which resulted in lower O_2 concentration in the rock layer. Consequently, the leaching of As by the oxidation of As-bearing minerals in the rock layer was reduced. Moreover, a longer water-resident time in the rock layer may induce precipitation of Fe oxy-hydroxide/oxide. These results suggest that the geochemical conditions of the rock layer affect As leaching and migration.

Keywords Arsenic, Leaching, Adsorption, Hydrothermally altered rock, Column experiments

1 Introduction

Arsenic (As) is a metalloid classified as a toxic substance at high concentrations. It can cause various kinds of human health problems, including acute and chronic toxicities depending on the dose (Chen et al. 1992; O'day et al. 2004). Arsenic is naturally found only in trace amounts. However, it can be concentrated in certain types of rocks, such as hydrothermally altered rocks. Hydrothermally altered rocks refer to rocks that have undergone an alteration by geothermal fluids, causing them to commonly contain arsenic-bearing minerals (Pirajno 2009). Exposure of these types of rocks to oxygen (O_2) and water leads to a potential source of As contamination of soil and groundwater.

In Hokkaido, Japan, rocks excavated by tunnel construction usually contain hydrothermally altered rocks (Takahashi et al. 2011; Tabelin et al. 2012a). Thus, as a result of

improper disposal, leachates containing high concentrations of As can be generated and may contaminate the surrounding environment, in particular groundwater and soil. Currently, the excavated rocks are often disposed in specially designed landfills (Katsumi et al. 2001). However, they are economically infeasible. Therefore, investigation into the factors controlling the mobility of As is required to design alternative disposal techniques of these potentially hazardous waste rocks.

The mobility of As from hydrothermally altered rocks is generally governed by precipitation, dissolution, adsorption, and desorption reactions, which are highly pH- and redox-dependent (Appelo and Postma 2005; Foster et al. 1998; Savage et al. 2000; Tabelin and Igarashi 2009). In our previous studies, we have reported the parameters controlling the mobility of As from hydrothermally altered rocks by using laboratory column experiments to mimic the actual disposal (Tabelin et al. 2012a, b, 2014). However, the relationship between the conditions of the columns, such as O_2 concentration and water content, and As leaching was not well described by those experimental setups. These two parameters may act as the fundamental key components of As release (Tabelin and Igarashi 2009; Tabelin et al. 2012a). Therefore, a more in-depth understanding of the mechanisms is still needed since it can be applied to the development of countermeasures that can be used to minimize the mobility of As from hazardous waste rocks. Herein, we have developed a method to demonstrate the effects of water content and O_2 concentration in relation to adding covering and adsorption layers on As leaching by introducing water content and O_2 concentration sensors into columns. By using the laboratory columns, O_2 concentration and water content were continuously monitored while simulated rain was irrigated. This study will allow a better understanding of As migration mechanisms from the rocks together with the development of disposal techniques for hazardous waste rocks.

2 Materials and Methods

2.1 Sample Collection and Preparation

The rock sample used in this study was collected from an interim storage site of a tunnel construction in Nakakoshi, Hokkaido, Japan. The rock had been stored in impoundment for about 6 months before sampling to determine the final disposal because the hydrothermally altered rock contained As. The bulk-excavated rock sample was taken by shovels at random points. The particle size ranged from about 20 cm (large particle) to <2 mm (fine particle) in diameter, and the bulk-excavated rock refers to the mixture of altered and unaltered rocks. In practice, during excavation, transportation, interim impoundment, and final disposal, the excavated rock can be naturally crushed into smaller particles. Therefore,

in preparation, the rock was air-dried under ambient conditions, crushed by a jaw crusher, sieved with a 2-mm aperture screen, and completely mixed to have a similar distribution of the particle size in columns to conservatively evaluate the risk. Finally, the sample was kept in air-tight containers to minimize oxidation.

Two natural geologic materials, river sediment and volcanic ash, were used as covering and adsorption layers. The river sediment was taken from a river located near the waste rock storage site while the volcanic ash came from the central part of Hokkaido. Sampling was also done by using shovels at random points. The same preparation process as the waste rock sample was also applied to these natural geologic materials.

2.2 Solid Sample Characterization

Pressed samples of finely crushed powder (<50 μm in diameter) of the rock and natural geologic materials were prepared for chemical and mineralogical analysis by X-ray fluorescence spectrometer (XRF) (Spectro Xepos, Rigaku Corporation, Japan) and X-ray diffractometer (XRD) (MultiFlex, Rigaku Corporation, Japan). The organic carbon (OC) content was obtained using the total carbon (TC) content and inorganic carbon (IC) content. The TC and IC were analyzed using a total carbon analyzer together with a solid sample combustion unit (TOC-VCSH-SSM-5000A, Shimadzu Corporation, Japan). The surface charges of the river sediment and volcanic ash were measured using Nano-ZS-60 (Malvern Instruments, UK), and the pH was adjusted by 0.1 M hydrochloric acid (HCl) or 0.1 M sodium hydroxide (NaOH).

2.3 Column Experiments

2.3.1 Apparatus

Figure 1 illustrates the laboratory column setup and dimensions of the columns. These columns were placed under ambient conditions to mimic the actual disposal environment. The columns, rainfall simulators, and stand were made of transparent polyvinyl chloride. All the columns were vertically mounted on the top of the stand and covered with the rainfall simulator. The covers were designed to have small holes for simulating actual rainfall and to protect the surface of the column from dust.

2.3.2 Column Setup

The physical properties of the packed layers are listed in Table 1. The packing of the

crushed rock sample in all the columns was standardized by compacting 679 g of the air-dried rock to a thickness of 5 cm. In the cases of columns with additional layer(s), the river sediment or volcanic ash was packed to a bulk density of 1.35 g/cm^3. Three sensors were installed inside each column. Two of them were responsible for measuring volumetric water content (Θ) (WD-3, ARP Corporation, Japan), and the other sensor was used for detecting O_2 concentration (MIJ-03, Environmental Measurement Japan Corporation, Japan). The O_2 concentration sensor was placed between the two water content sensors, which were located at a depth of 5 and 15 cm from the top of the crushed rock layer as shown in Fig. 1. These sensors simultaneously recorded the data every 10 min and sent the real-time change of data to a data logger (FT2-CTRL, M.C.S. Corporation, Japan) throughout the experiments.

2.3.3 Irrigation and Collection of Effluent

Distilled water was irrigated via a rainfall simulator to mimic actual rain. Every week, 200 mL of distilled water, equivalent to the average rainfall in Hokkaido, was poured at once to the rain fall simulator at the top of each column, and it gravitationally infiltrated to the packed layer, representing a heavy rainfall (Ministry of Land Infrastructure Transport and Tourism Japan 2010). This irrigation corresponds to the worst case scenario in terms of As leaching (Tabelin et al. 2012a). Effluents were collected at the bottom of each column by using a 250-mL polypropylene bottle. Since the columns were initially dried, a time lag between the first irrigation and the first collection was observed. In case 1, the first effluent sample was collected on the 3rd week. In contrast, in cases 2, 3, and 4, the first effluents were obtained in the 4th week. The longer time lag was observed in cases 2, 3, and 4 because of the presence of additional layer(s) resulting in larger pore volume (PV) or larger space for holding the irrigated water. After the first collection, effluents were regularly collected once a week before the next irrigation. Once obtained the effluents, pH, ORP, and EC of the liquid sample were immediately measured, then filtered using 0.45-μm Millex® filters, and stored in an air-tight polypropylene bottle prior to chemical analysis.

2.4 Chemical Analysis of Effluents

Inductively coupled plasma atomic emission spectrometer (ICP-AES) (ICPE-9000, Shimadzu Corporation, Japan) was used to quantify the concentration of elements. A hydride generation technique was applied to determine As concentration. This technique required a process of pre-treatment in which 10 mL of sample was mixed with 3 mL of 12 M HCl, 0.66 mL of 20% of potassium iodide solution, 0.33 mL of 10% of ascorbic acid solution, and 0.66 mL of deionized water (Tabelin et al. 2012b). Reagent-grade chemicals were used in the analysis. Note that an error of 2–3% was found in ICP-AES while the hydride generation technique

had 5% inaccuracy. Concentrations of coexisting ions were quantified by cation and anion chromatographs (ICS-1000, Dionex Corporation, USA). Bicarbonate ion (HCO_3^-) was analyzed by titration with 0.01 M sulfuric acid (H_2SO_4) solution.

3 Results and Discussion

3.1 Properties of Solid Samples

Chemical composition and mineral constituents of the bulk-excavated rock, river sediment, and volcanic ash are listed in Tables 2 and 3, respectively. The content of As in the bulk-excavated rock was 23.6 mg/kg, which is two times higher than the global average content in sedimentary rocks (Webster 1999). This confirms that this waste rock can potentially release significant amounts of As into the environment. The majority of As resulted from geothermal fluid alterations (Takahashi et al. 2011). Many different types of minerals were identified in the rock as illustrated in Table 3. The rock was composed of quartz as a primary mineral; feldspar as the second highest; minor minerals of calcite, chloride, and kaolinite; and a trace amount of pyrite. The presence of calcite can affect the pH of leachate because dissolution of calcite generates HCO_3^-, which becomes a buffer solution (Deutsch 1997; Morse et al. 2007). Even though a trace amount of pyrite was found in the excavated rock, oxidation of pyrite can be suspected as a major source of As. This assumption was made from the fact that pyrite was oxidized after exposure to the atmosphere, and therefore, most of the exchangeable fraction in the rock probably originated from the oxidation of pyrite during the exposure to the environment for about 6 months before sampling (Schaufuß et al. 1998). On the other hand, the As content in the river sediment was low and close to the average content of geogenic As (Smedley and Kinniburgh 2002). In contrast, the volcanic ash contains the highest amount of As among all solid samples. The majority of As was found in the residual phase, which was not likely to leak. This fact was confirmed by a very low leaching concentration of As (<1 μg/L) in the batch leaching test. The river sediment and volcanic ash mainly contained silicate mineral with substantial amounts of Al_2O_3 and Fe_2O_3, having an adsorption potential for removing As (Ghosh and Yuan 1987; Wang and Mulligan 2006; Cornelis et al. 2008).

The physical properties of the solid samples are summarized as listed in Table 1. These samples were classified as a semi-permeable material because the hydraulic conductivity was in the range of 10^{-5}–10^{-6} m/s, suggesting that the volcanic ash and river sediment are ideal to be used as covering and adsorption layers in terms of permeability. Figure 2 shows the results of the zeta potential of the river sediment and volcanic ash as a function of pH. Although the river sediment and volcanic ash had negative surface charge in a

wide range of pH (2–12), these two samples were selected as an adsorption layer.

3.2 Effects of Additional Layer(s) on Water Content and Oxygen Concentration

Figures 3a–d show the change in volumetric water content in cases 1 to 4. Some missing points of water content in case 1 were observed due to a sensor failure. Water content in all the columns was initially around 0.2 since the air-dried samples were packed. During the first few weeks, after irrigation in all the cases, the water content rapidly increased, and then remained at higher water content of around 0.3 to 0.4, demonstrating the accumulation of water inside the columns. The water content at a deeper rock layer in case 1 was slightly decreased after each irrigation for the first few weeks whereas the water content in the other cases became almost constant regardless of the irrigation. This is probably due to the water retention characteristics of additional layer(s) in cases 2 to 4; covering and adsorption layers can help to prevent rapid evaporation and percolation of water from the rock layer, respectively.

The average evaporation rate was determined by the mass balance calculation as shown in Equation (1).

Evaporation rate = 200 - mass of effluent (ml/week) (1)

The calculation was done at the point where water was no longer accumulated inside the columns. In case 2, the result cannot be obtained due to the development of clogging water pathways in the column. The average evaporation rate in case 1 was 14.5 mL/week. In contrast, the rate was reduced to 9.6 and 12.2 mL/week in cases 3 and 4, respectively. These results indicate the reduction of evaporation by the covering layer. Although the highest evaporation rate was found in case 1, it was still low and insignificant compared to the weekly irrigation (200 mL).

In all the columns, as time elapsed, the shallower water content fluctuated in accordance with weekly irrigation while almost constant water content was observed in the deeper layer. These results indicate that the water content in the upper rock layer was unsaturated whereas the water content in the lower layer was almost saturated. Generally, the volumetric water content in the shallower layer should not exceed the content in the deeper layer. However, the inverse trend can be seen in some data points of cases 1 and 2 (Fig. 3a, b). This was probably due to the looser packing of rock around the shallower sensors when fixing the sensors in the columns. The degree of fluctuation of the shallower water content in case 3 was less drastic than those in cases of 1, 2, and 4, probably due to the lower porosity around the sensor. However, the nearly saturated zone in the deeper rock layer was expected

to be more significant in cases 2, 3, and 4 than case 1 due to the presence of the adsorption layer in those cases. Moreover, in case 2, a flat peak of the signal from the shallower sensor was observed from week 9, indicating larger development of the zone with almost saturated water content, caused by development of clogging water pathways in the column.

Figure 4 shows the change in O_2 concentration in cases 1 to 4. The O_2 sensors used in this experiment can detect O_2 concentration in both gaseous and aqueous phases. Initial O_2 concentration was approximately 21% in all the cases, which is equivalent to the average ambient concentration of O_2. Except for case 1, the amount of O_2 gradually decreased before the first collection. After the water content at the deeper rock layer approached saturation, O_2 concentration dramatically decreased and reached almost zero at week 6 in cases 2 and 3, and at week 10 in case 4. On the other hand, in case 1, O_2concentration gradually decreased until week 10 before exponentially decreasing and reaching almost zero at week 15. These results clearly indicate a negative correlation between O_2 concentration and volumetric water content, meaning that the faster the accumulation of water, the faster the reduction of O_2 concentration. A delay in the reduction among them was observed, which is possibly due to the effects of the adsorption and covering layers. It was only the rock layer in case 1 (without covering and adsorption layers) that led to the slowest accumulation of water among all the cases. This resulted in high O_2 concentration during the first 10 weeks before decreasing to almost zero. Moreover, the O_2 concentration was affected not only by water replacement but also by the oxidation of sulfide minerals in the rock. This observation was supported by the slight reduction of O_2 concentration at the position where water content was already stable.

3.3 Effects of Additional Layer(s) on pH, Eh, EC, and Coexisting Ions

The pH values in all the cases ranged between neutral and moderately alkaline as shown in Fig. 5a. This variation in pH could be mainly attributed to three processes, including pyrite oxidation, precipitation of Fe oxy-hydroxide/oxide, and dissolution of calcite.

The aqueous pyrite oxidation generally occurs according to the following chemical equations (Chandra and Gerson 2010):

$$FeS_2(s)+7/2O_2(aq)+H_2O \Leftrightarrow Fe^{2+}+2H^{+}+2SO_4^{2-} \quad (2)$$

$$FeS_2(s)+14Fe^{3+}+8H_2O \Leftrightarrow 15\ Fe^{2+}+16H^{+}+8\ SO_4^{2-} \quad (3)$$

Under neutral and moderately alkaline pH, ferrous (Fe^{2+}) is rapidly oxidized to ferric

(Fe^{3+}), and then precipitated as Fe oxy-hydroxide/oxide according to the following reactions (Stumm and Lee 1961; Gupta and Gupta 2005):

$$Fe^{2+}+1/4\ O_2\ (aq)+H^{+}\Leftrightarrow Fe^{2+}+1/2H_2O \quad (4)$$

$$Fe^{3+}+3H_2O\Leftrightarrow Fe(OH)_3\ (s)+3H^{+} \quad (5)$$

Therefore, pyrite oxidation and precipitation of dissolved Fe are the reactions to lowering the pH of the effluent.

However, calcite dissolution (Equation (6)) consumes H^{+} and generates HCO_3^{-}, which has a buffering capacity as a by-product (Lui and Dreybrodt 1997). Therefore, neutral to moderately alkaline pH was observed in all the cases.

$$CaCO_3(s)+H^{+}\Leftrightarrow Ca^{2+}+HCO_3^{-} \quad (6)$$

In cases 1 and 4, the variation of pH was relatively stable ranging between 7.6 and 8.4 throughout the experiment except the pH of the first effluent in case 4. On the other hand, in cases 2 and 3, the pH of effluents was initially low, and then slightly increased and stabilized at around pH 8.2–8.4. Thus, the pH buffering capacity of the volcanic ash and river sediment reduced the pH in cases 2, 3, and 4 at the beginning of the experiment.

In all the cases, Eh was relatively uniform, ranging between 325 and 475 mV as shown in Fig. 5b. Thus, the presence of the additional layer(s) did not have a significant effect on the variability of Eh.

Figures 5c, d illustrate the leaching behavior of calcium ion (Ca^{2+}) and sulfate ion (SO_4^{2-}), respectively. In all the cases, the concentrations of Ca^{2+} and SO_4^{2-} were high at first and dramatically decreased before becoming steady. The leaching curve of Ca^{2+} stabilized at around 148, 40, 48, and 115 mg/L in cases 1, 2, 3, and 4, respectively. On the other hand, the concentration of SO_4^{2-} stabilized at the average values of 252, 55, 77, and 176 mg/L. The variation of EC in all the cases was highly correlated with the Ca^{2+} and SO_4^{2-} leaching concentrations as shown in Fig. 6a, b, respectively. These correlations suggest that the majority of ions contained in the effluents were Ca^{2+} and SO_4^{2-}. Therefore, the flushing-out trends of these ions resulted from calcite dissolution and pyrite oxidation together with the dissolution of soluble phase minerals such as Ca-sulfates (e.g., gypsum) and Fe-sulfates ($Fe_2(SO_4)_3$, Fe SO_4), most likely caused by calcite dissolution and pyrite oxidation before sampling (Chandra and Gerson 2010; Donato et al. 1993; Todd et al. 2003). The stable and

low leaching curves of those ions were probably due to the continuation of calcite dissolution and pyrite oxidation. Figure 7 illustrates the relationship between molar concentration of SO_4^{2-} and that of Ca^{2+} in the effluent of case 1. The correlation was made at the points where the leaching curves of those ions were stable to avoid the effects of the dissolution of soluble phase minerals. A positive correlation with a molar ratio between SO_4^{2-} and Ca^{2+} of approximately 0.5 was observed. This result indicates that the calcite dissolution and pyrite oxidation occurred simultaneously by ignoring the Equation (3) because of weakly alkaline conditions. It can also be confirmed by the relatively stable pH in case 1 since the dissolution of calcite generates HCO_3^-, having a buffering capacity to resist lowering pH due to pyrite oxidation (Fig. 5a).

The concentration of SO_4^{2-} in case 1 was the highest during most of the experimental period. This result suggests lower oxidation of pyrite in cases 2, 3, and 4, meaning that the presence of covering and adsorption layers and/or a faster and larger development of the nearly saturated zone in the rock layer plays a role in reducing pyrite oxidation in the rock layer. The lower oxidation of pyrite results from the depletion of aqueous O_2 in the rock layer, caused by a lower diffusion of air. As more water accumulates inside the rock, it slows down the air diffusion rate, thereby reducing its O_2 load (Aachib et al. 2004; Bornstein et al. 1980; Neira et al. 2015). However, the covering layer did not dramatically influence the pyrite oxidation since the SO_4^{2-} concentration in case 2 was almost identical to that in case 3. This means that the effects of the covering layer on lowering the air diffusion rate was less significant compared to the effects of water accumulation in the rock layer. The reduction in pyrite oxidation might lower calcite dissolution since H^+, the product of pyrite oxidation, can be the reactant dissolving calcite (Equation (5)). However, the leaching of Ca^{2+} was mainly controlled by the adsorption of Ca^{2+} onto the surface of the adsorption layer due to the negative surface charge. This was confirmed by the highest Ca^{2+} concentration in case 1.

3.4 Effects of the Additional Layer(s) on Arsenic Release

Figure 8 shows the change of As concentration in the effluent in cases 1 to 4. The As concentration in case 1 was the highest among all the cases and fluctuated between 19 and 38 μg/L throughout the experiment. On the other hand, the leaching concentration of As in case 4 was higher than 10 μg/L during the first 17 weeks before a sudden decrease in week 19 to below 5 μg/L while, in cases of 2 and 3, it was below the drinking water guideline (10 μg/L) except for the leaching of the second effluent in case 2 (WHO 2011). Figure 9 illustrates the correlation between As concentration in the effluents and pH of cases 1 to 4. A positive correlation was observed in case 1 while the opposite trend was found in the other cases. In

general, As tends to desorb and become harder to adsorb with increasing pH since surface charges of adsorbents turn to be more negative (Dzombak and Morel. 1990). However, in cases 2 to 4, the negative correlation was obtained, which is due to the role of additional layer(s). As mentioned earlier, the presence of additional layer(s) resulted in faster and larger development of the nearly saturated zone in the rock layer. This plays an important role in reducing the mobilization of As because of the following mechanisms: first, when the water was accumulated within the rock layer, it led to a slower diffusion rate of O_2 into the rock layer, and second, the lower O_2 concentration decreased oxidation of sulfide minerals, especially pyrite, which resulted in less As released from the rock. Although the adsorption materials had a negative surface charge, these materials also contributed to the reduction of As levels because they contained substantial amounts of Al_2O_3 and Fe_2O_3 and their own buffering capacity to lower the pH, resulting in increasing As adsorption by the development of a positive surface charge on the adsorbent. The role of the covering layer is generally to limit the intrusion of water and O_2 from the surroundings into the rock. However, it could not be clearly determined since the effects of water runoff were restricted by using one-dimensional column experiments. Moreover, the movement of water in the rock layer may also be a potential factor affecting the migration of As. In cases 2 and 3, the longer water retention time in the rock layer caused by lower hydraulic conductivity of the adsorption layer may lead to more precipitation of Fe oxy-hydroxide/oxide. Longer water residence time allows more time for water to dissolve Fe from the dissolvable phase (e.g., $Fe_2(SO_4)_3$) and precipitate as Fe oxy-hydroxide/oxide, producing H^+ as a by-product. This might be the result of a very low amount of As leaching in cases 2 and 3 due to the following reasons: the first is that these precipitates have high adsorption affinities toward As (Safiullah et al. 2004; Tabelin et al. 2012a), the second is that As can also be co-precipitated with Fe oxy-hydroxide/oxide (Klerk et al. 2012; Ruiping et al. 2007), and the third is that the higher amounts of these precipitates result in a lower pH, which also enhances the As adsorption.

4 Conclusion

Four cases of laboratory column experiments were carried out. The replacement of air by water led to a negative correlation between volumetric water content and O_2 concentration. The presence of additional layer(s) led to faster and larger development of the zone with higher water content since rapid evaporation and percolation of water from the rock layer were limited by the covering and adsorption layers, respectively. This process resulted in the reduction of oxidation of As-bearing minerals due to slower diffusion of air into pore water. In addition, As was also retarded by the adsorption layer located underneath the rock layer since it contained substantial amounts of Fe and Al oxide. Moreover, a lower water flow rate induced by the use of covering and adsorption layers with lower hydraulic

conductivity compared with the rock layer may lead to higher precipitation of Fe oxy-hydroxide/oxide in the adsorption layer, which has a strong adsorption affinity to As. As a result, the columns with additional layer(s) released significantly lower amounts of As.

Acknowledgements

Part of this research was supported by the Japan Society for the Promotion of Science (JSPS) grant-in-aid for scientific research (grant number 26289149).

References

Aachib, M., Mbonimpa, M., Aubertin, M. (2004). Measurement and prediction of the oxygen diffusion coefficient in unsaturated media, with applications to soil covers. Water, Air, & Soil Pollution, 156(1), 163–193.

Appelo, C. A. J., Postma, D. (2005). Geochemistry, Groundwater and Pollution (2nd. ed.). London: A.A. Blkema. Bornstein, J., Hedstrom, W. E., Scott, F. R. (1980). Oxygen diffusion rate relationships under three soil conditions. Technical Bulletin, 98, 1–12.

Chandra, A. P., Gerson, A. R. (2010). The mechanisms of pyrite oxidation and leaching: A fundamental perspective. Surface Science Reports, 65(9), 293–315.

Cornelis, G., Johnson, C. A., Gerven, T. V., Vandecasteele, C. (2008). Leaching mechanisms of oxyanionic metalloid and metal species in alkaline solid wastes: A review. Applied Geochemistry, 23(5), 955–976.

Deutsch, W. J. (1997). Groundwater Geochemistry: Fundamentals and Applications to Contamination. Florida: Lewis.

Donato, P., Mustin, C., Benoit, R., Erre, R. (1993). Spatial distribution of iron and sulphur species on the surface of pyrite. Applied Surface Science, 68(1), 81–93.

Dzombak, D. A., Morel, F. M. M. (1990). Surface Complexation Modeling: Hydrous Ferric Oxide. New York: Wiley.

Foster, A. L., Brown, G. E. Jr., Tingle, T. N., Parks, G. A. (1998). Quantitative arsenic speciation in mine tailings using X-ray absorption spectroscopy. American Mineralogist, 83,

553–568.

Ghosh, M. M., Yuan, J. R. (1987). Adsorption of inorganic arsenic and organoarsenicals on hydrous oxides. Environmental Progress, 6(3), 150–157.

Gupta, A. K., Gupta, M. (2005). Synthesis and surface engineering of iron oxide nanoparticles for biomedical applications. Biomaterials, 26(18), 3995–4021.

Katsumi, T., Benson, C. H., Foose, G. J., Kamon, M. (2001). Performance-based design of landfill liners. Engineering Geology, 60(1-4), 139–148.

Klerk, R. J. D., Jia, Y., Daenzer, R., Gomez, M. A., Demopoulos, G. P. (2012). Continuous circuit coprecipitation of arsenic (V) with ferric iron by lime neutralization: Process parameter effects on arsenic removal and precipitate quality. Hydrometallurgy, 111–112, 65–72.

Lui, Z., Dreybrodt, W. (1997). Dissolution kinetics of calcium bcarbonate minerals in H_2O–CO_2 solutions in turbulent flow: The role of the diffusion boundary layer and the slow reaction

$H_2O + CO_2 \leftrightarrow H^+ + HCO_3^-$. Geochimica et Cosmochimica Acta, 61, 2879–2889.

Marumo, K., Ebashi, T., Ujiie, T. (2003). Heavy metal concentrations, leachability and lead isotope ratios of Japanese soils. Shigen Chisitsu 53 (2), 125-146 (in Japanese with English abstract).

Ministry of Land Infrastructure Transport and Tourism Japan (2010). Status of water resources in Japan. http://www.mlit. go.jp/common/001121771.pdf, Accessed 1 September 2016.

Morse, W. J., Arvidson, S. R., Luttge, A. (2007). Calcium carbonate formation and dissolution. Chemical Reviews, 107(2), 342–381.

Neira, J., Ortiz, M., Morales, L., Acevedo, E. (2015). Oxygen diffusion in soils: Understanding the factors and processes needed for modeling. Chilean Journal of Agricultural Research, 75, 35–44.

Ruiping, L., Xing, L., Shengji, X., Yanling, Y., Rongcheng, W., Guibai, L. (2007). Calcium-enhanced ferric hydroxide coprecipitation of arsenic in the presence of silicate. Water Environment Research, 79(11), 2260–2264.

Safiullah, S., Kabir, A., Hasan, K., Rahman, M. M. (2004). Comparative study of adsorption-desorption of arsenic on various arsenic removing materials. Journal of Bangladesh
Academy of Sciences, 28(1), 27–34.

Savage, K. S., Tingle, T. N., O'day, P. A., Waychunas, G. A., Bird, D. K. (2000). Arsenic speciation in pyrite and secondary weathering phases, Mother Lode Gold District, Tuolumne Country, California. Applied Geochemistry, 15(8), 1219–1244.
Schaufuß, A. G., Nesbitt, H. W., Kartio, I., Laajalehto, K., Bancroft, G. M., Szargan, R. (1998). Reactivity of surface chemical states on fractured pyrite. Surface Science, 411,
321–328.

Smedley, P. L., Kinniburgh, D. G. (2002). A review of the source, behavior and distribution of arsenic in natural waters. Applied Geochemistry, 17(5), 517–568.

Stumm, W., Lee, F. (1961). Oxygenation of ferrous iron. Industry and Engineering Chemistry, 53, 143–146.

Tabelin, C. B., Igarashi, T. (2009). Mechanisms of arsenic and lead release from hydrothermally altered rock. Journal of Hazardous Materials, 169(1-3), 980–990.

Tabelin, C. B., Igarashi, T., Takahashi, R. (2012a). Mobilization and speciation of arsenic from hydrothermally altered rock in laboratory column experiments under ambient conditions.
Applied Geochemistry, 27(1), 326–342.

Tabelin, C. B., Igarashi, T., Yoneda, T. (2012b). Mobilization and speciation of arsenic from hydrothermally altered rock containing calcite and pyrite under anoxic conditions. Applied Geochemistry, 27(12), 2300–2314.

Tabelin, C. B., Igarashi, T., Arima, T., Sato, D. (2014). Characterization and evaluation of arsenic and boron adsorption onto geologic materials, and their application in the disposal of excavated altered rock. Geoderma, 213, 163–172.

Takahashi, T., Fujii, K., Igarashi, T., Kaketa, K., Yamada, N. (2011). Distribution properties and leaching of arsenic by the hydrothermally-altered rocks of Nakakoshi Area, central Hokkaido, Japan. Journal of the Japan Society of Engineering Geology, 52(2), 46–54.

Todd, E. C., Sherman, D. M., Purton, J. A. (2003). Surface oxidation of pyrite under ambient atmospheric and aqueous (pH = 2 to 10) conditions: Electronic structure and mineralogy from X-ray absorption spectroscopy. Geochimica et Cosmochimica Acta, 67(5), 881–893.

Wang, S., Mulligan, C. N. (2006). Natural attenuation processes for remediation of arsenic contaminated soils and groundwater. Journal of Hazardous Materials, 138(3), 459–470.

Webster, J. G. (1999). Arsenic. In C. P. Marshall & R. W. Fairbridge (Eds.), Encyclopedia of geochemistry (pp. 21–22). London: Chapman Hall.

WHO (World Health Organization) (2011). Guidelines for drinking-water quality. 4th. edition.

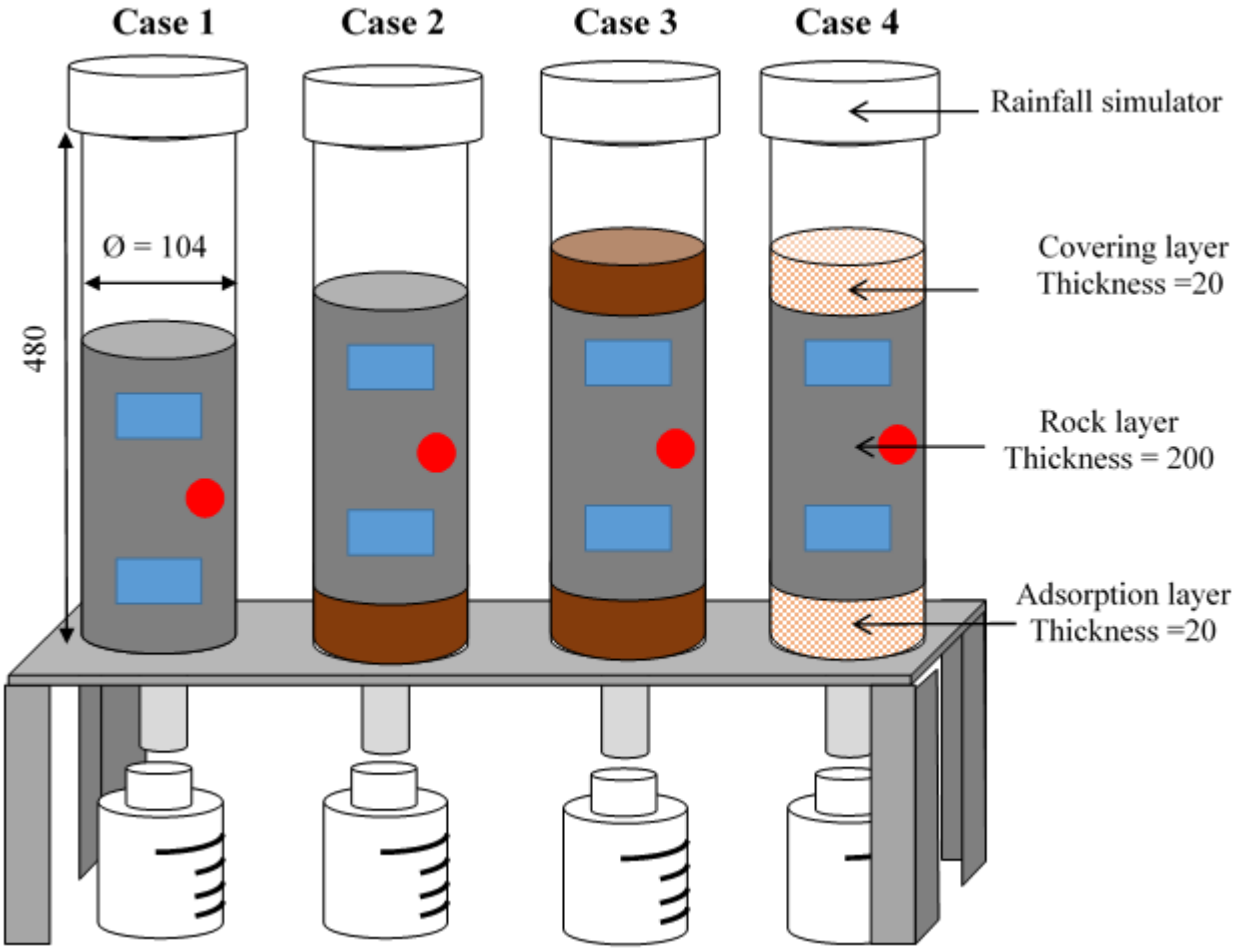

Figure 1 Schematic of the columns; ( ) Oxygen concentration sensor, ( ) Water content sensor, ( ) volcanic ash, and ( ) river sediment (All units are in mm.)

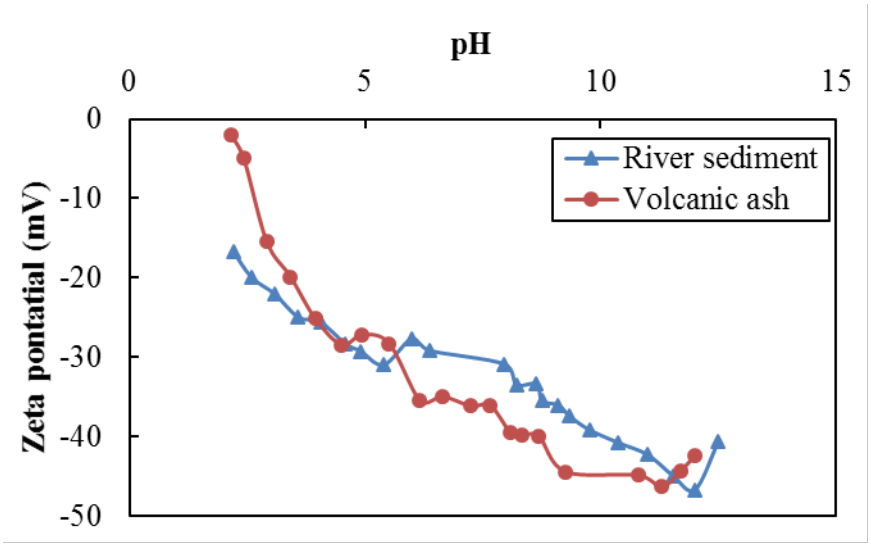

Figure 2 Zeta potential vs pH of river sediment and volcanic ash

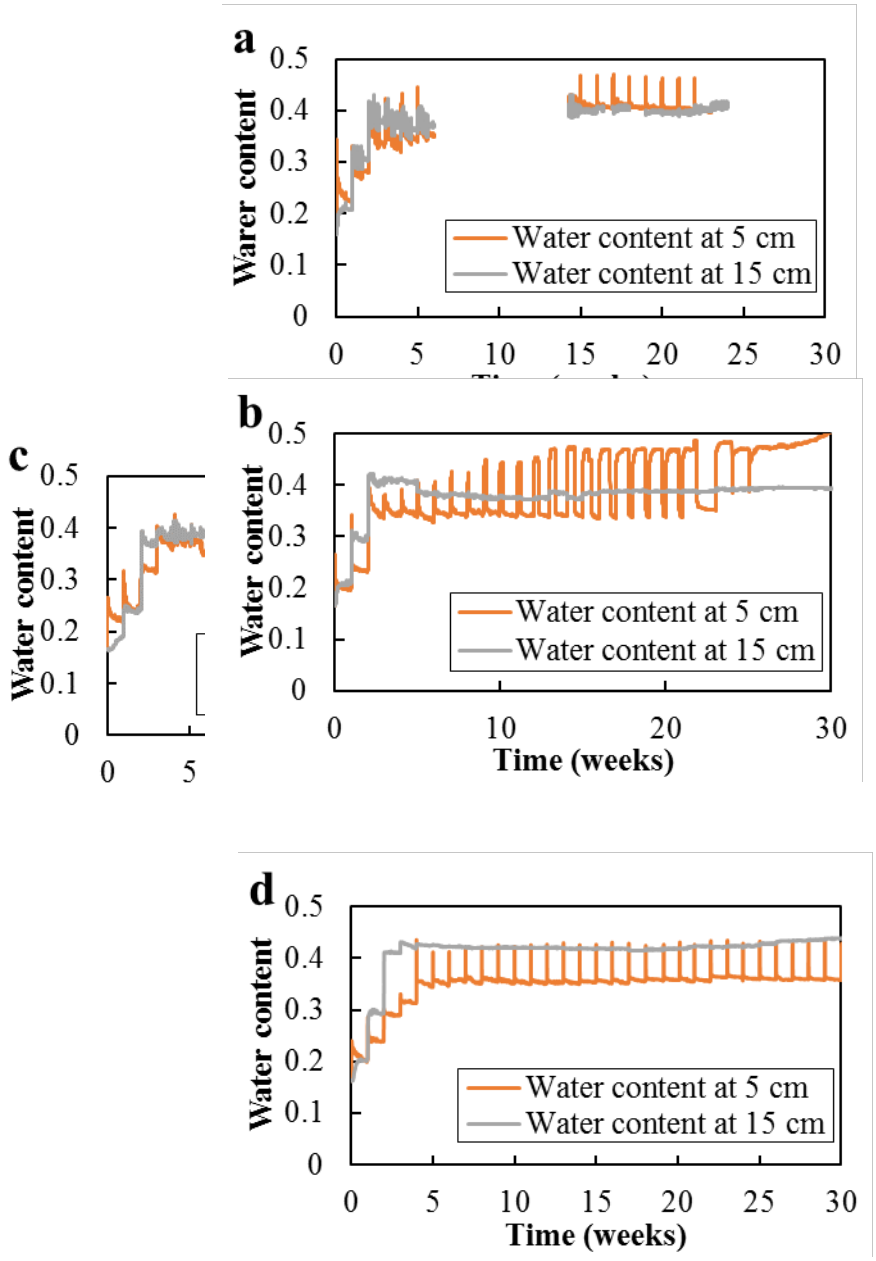

Figure 3 Changes in water content; (a) Case 1, (b) Case 2, (c) Case 3, and (d) Case 4

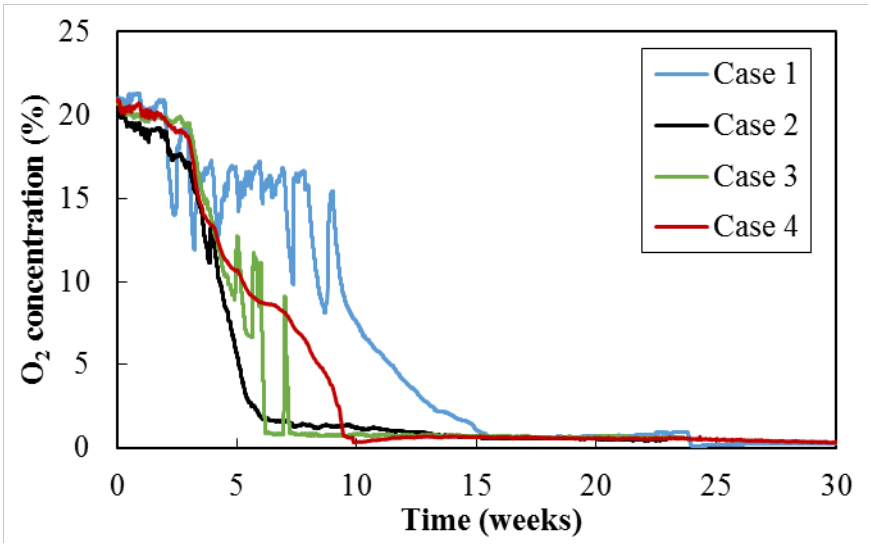

Figure 4 Changes of oxygen concentration

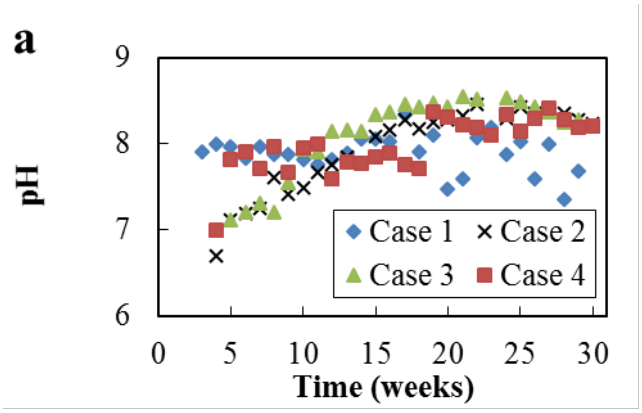

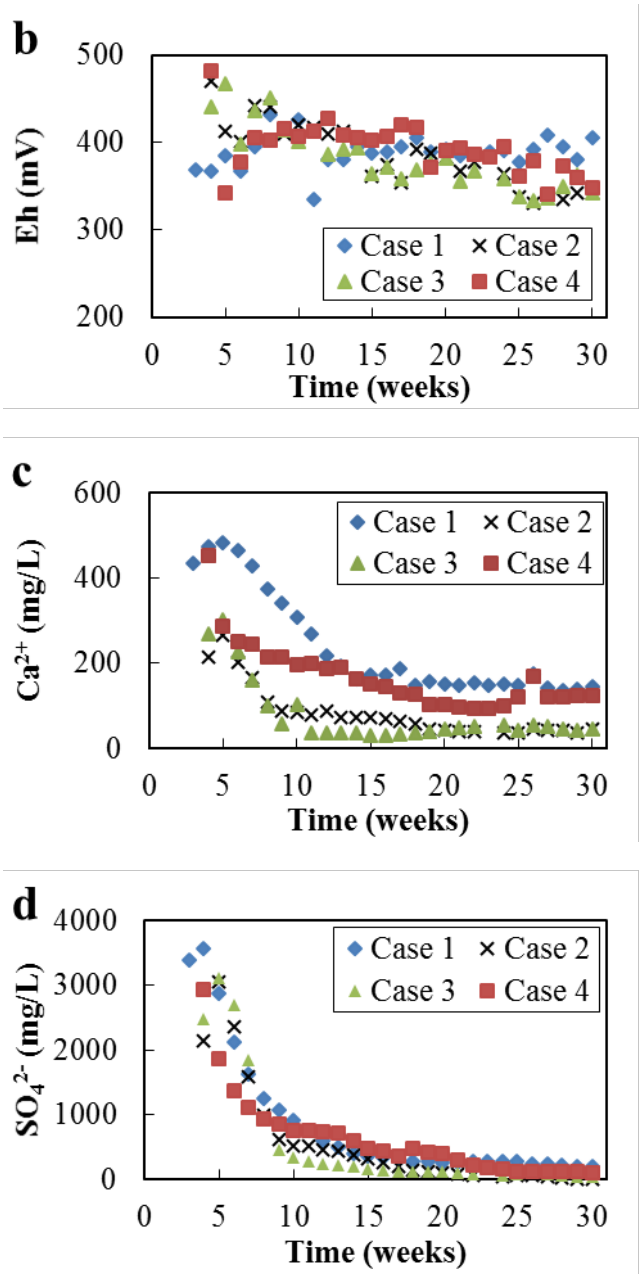

Figure 5 Changes in pH, Eh, Ca^{2+}, and SO_4^{2-} concentrations with time; (a) pH vs time, (b) Eh vs time, (c) Ca^{2+} concentration vs time, and (d) SO_4^{2-} concentration vs time

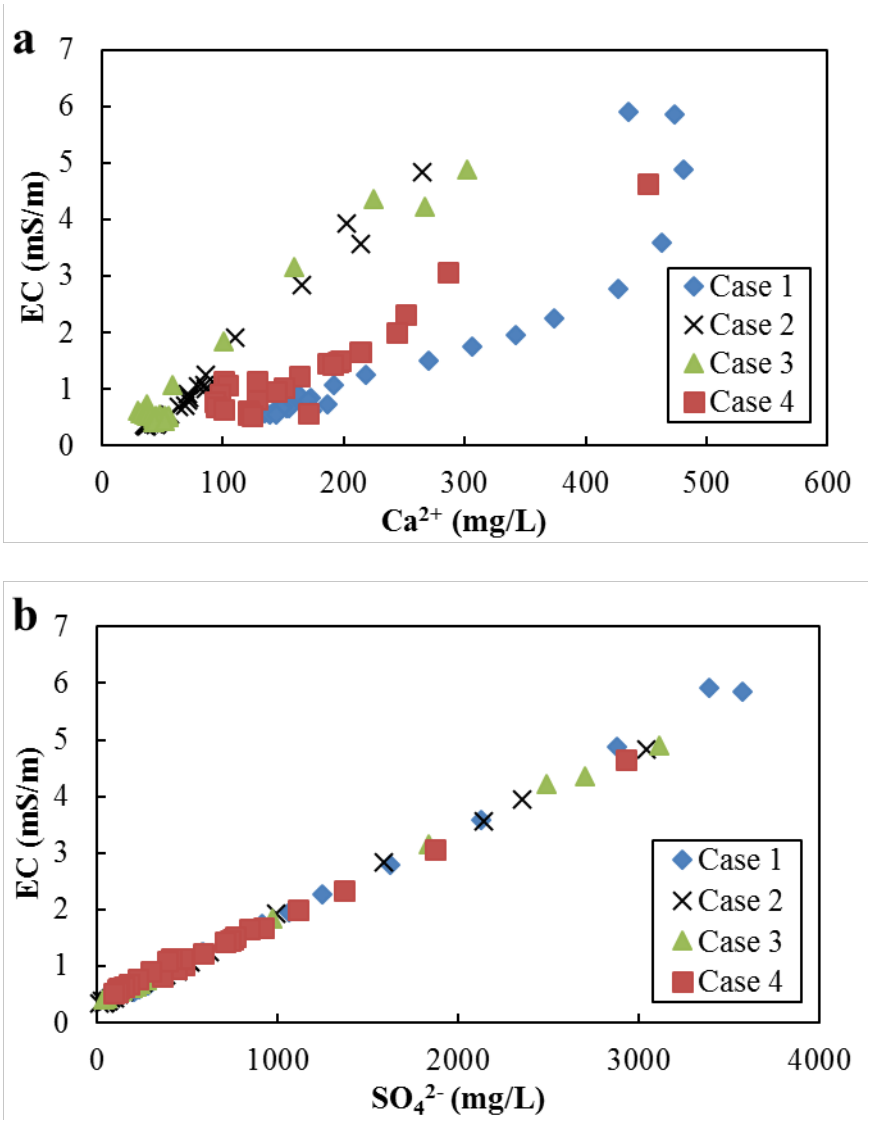

Figure 6 Electrical conductivity vs concentrations of (a) Ca^{2+} and (b) SO_4^{2-}

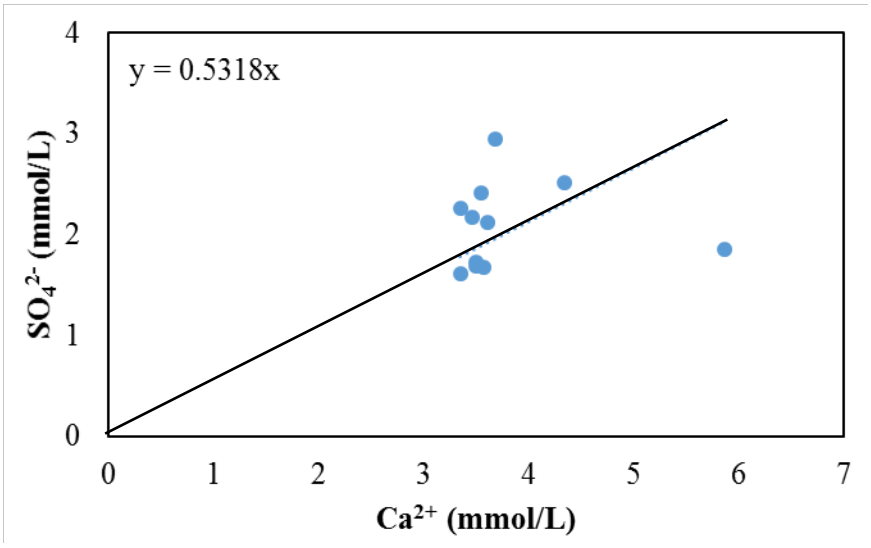

Figure 7 Correlation between SO_4^{2-} and Ca^{2+} in case 1

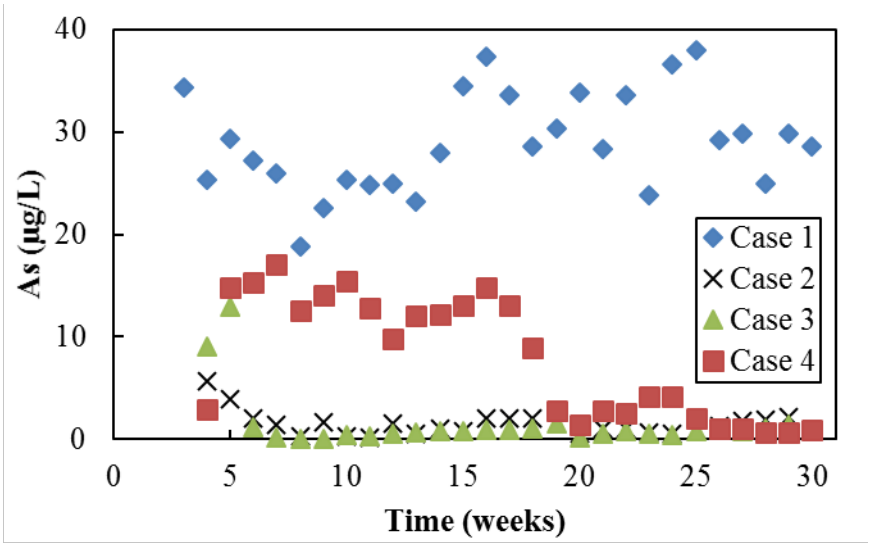

Figure 8 Changes in As concentration with time

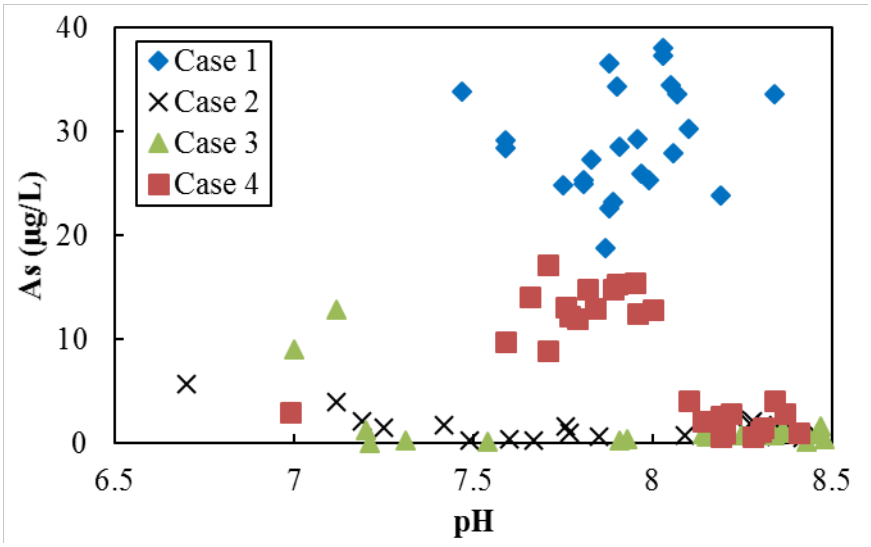

Figure 9 As concentration vs pH

Table 1 Initial conditions of column experiments

Column number	Irrigation volume (ml/week)	Excavated rock layer			Additional layer(s)					
		Bulk density (Air-drying) (g/cm^3)	Porosity (%)	Hydraulic conductivity (m/s)	Material	Bulk density (Air-drying) (g/cm^3)	Porosity (%)	Hydraulic conductivity (m/s)	Covering layer	Adsorption layer
1	200	1.62	41	6.8×10^{-6}	-	-	-		No	No
2	200	1.62	41	6.8×10^{-6}	Volcanic ash	1.35	55.8	1.68×10^{-6}	No	Yes
3	200	1.62	41	6.8×10^{-6}	Volcanic ash	1.35	55.8	1.68×10^{-6}	Yes	Yes
4	200	1.62	41	6.8×10^{-6}	River sediment	1.35	48.7	8.35×10^{-5}	Yes	Yes

Table 2 Chemical composition of bulk excavated rock, river sediment, and volcanic ash

	Rock	River sediment	Volcanic ash
SiO_2 (wt.%)	58.7	55.3	57.6
TiO_2 (wt.%)	0.82	0.81	0.9
Al_2O_3 (wt.%)	14.4	15.2	19.1
Fe_2O_3 (wt.%)	6.22	6.97	8.7
MnO (wt.%)	0.07	0.13	0.11
MgO (wt.%)	3.49	2.02	1.4
CaO (wt.%)	3.31	1.75	0.9
Na_2O (wt.%)	1.31	1.35	1.1
K_2O (wt.%)	3.22	1.73	1.3
P_2O_5 (wt.%)	0.13	0.07	0.029
S (wt.%)	0.2	< 0.01	< 0.01
As (mg/kg)	23.6	0.9	31.8
LOI (wt%)	6.26	6.3	8.99
Organic C (wt%)	0.23	< 0.01	< 0.01
Water (wt%)	1.10	1.12	2.23

Table 3 Mineralogical composition of rock sample, river sediment, and volcanic ash

	Excavated rock	River sediment	Volcanic ash
Quart	+++	+++	+++
Feldspar	++	++	++
Kaolinite	+		
Calcite	+		
Chlorite	+		+
Pyrite	-		
Cristobalite			+
Smectite			+

+++: High; ++: Medium; +: low; -: Trace.